JOURNAL OF GEOPHYSICAL RESEARCH, VOL. 106, NO. D12, PAGES 12,727–12,738, JUNE 27, 2001

Global stratospheric effects of the alumina emissions by solid-fueled rocket motors

M. Y. Danilin, R.-L. Shia, M. K. W. Ko, D. K. Weisenstein, and N. D. Sze

Atmospheric and Environmental Research, Inc., Lexington, Massachusetts

J. J. Lamb, T. W. Smith, and P. D. Lohn

TRW, Inc., Redondo Beach, California

M. J. Prather

University of California, Irvine, California

Abstract. We simulate accumulation of Al_2O_3 particles in the atmosphere produced by solid-fueled rocket motors by using the Goddard Institute for Space Studies/University of California at Irvine three-dimensional (3-D) chemistry-transport model (CTM). Our study differs from Jackman et al. (1998) by applying a 3-D CTM, considering 13 size bins for the emitted particles from 0.025 to 10 μm and taking into account their washout, gravitational sedimentation, and coagulation with background sulfate aerosol. We assume an initial trimodal size distribution of Al_2O_3 particles (Beiting, 1997) with 2.8% by mass of the alumina emitted as particles with radius of less than 1 μm. Our test case adopts a stratospheric source of 1120 tons/yr equivalent to nine space Shuttle and four Titan IV launches annually. The calculated steady state surface area density (SAD) and mass density for the scenarios with sedimentation of alumina particles have maximum values in the lower stratosphere in the Northern Hemisphere of up to 7×10^{-4} $\mu m^2/cm^3$ and 0.09 ng/m^3, respectively, or about 1000 times smaller than those of the background sulfate aerosol. Our results are sensitive to the emitted mass fractionation of alumina (EMFA) showing the values for the SAD or mass density higher or lower by an order of magnitude owing to a poorly known EMFA. Chemical implications of alumina particle accumulation for the ozone balance are estimated by using the Atmospheric and Environmental Research 2-D model assuming chlorine activation on Al_2O_3 surfaces via the $ClONO_2 + HCl \rightarrow Cl_2 + HNO_3$ reaction with a probability of 0.02 (Molina et al., 1997). Owing to the very small Al_2O_3 SAD, any additional ozone depletion due to Al_2O_3 emissions is also small (0.0028% on a global annually averaged basis for the scenario with sedimentation, or about 4 times smaller than the ozone response to chlorine emissions only). The ozone depletion potential of the alumina emissions is about 0.03-0.08 for the scenarios using the EMFA of Beiting (1997) and larger by an order of magnitude for the EMFA of Brady and Martin (1995).

1. Introduction

Fuel for solid-fueled rocket motors (SRMs) consists of NH_4ClO_4 (≈70% by weight), Al (≈16%), and binders (≈14%) [*Prather et al.*, 1990a], which, after burning, produces Al_2O_3 particles as a dominant component among other exhaust products. The main components of the space shuttle SRM exhaust are Al_2O_3 (30% by weight), CO (24%), HCl (21%), H_2O (10%), N_2 (9%), CO_2 (4%), and H_2 (2%) emitted up to 42 km [*Prather et al.*, 1990a]. The environmental impact of the SRM emissions has been examined [e.g., *World Meteorological Organization (WMO)*, 1992]. It is believed that chlorine emissions (mostly in the form of HCl and Cl_2) pose the main risk for the ozone layer compared with the other SRM emissions. On the global scale, the depletion of the ozone column caused by SRM chlorine emissions is very small (<0.1% at northern midlatitudes and about 0.01% over the globe assuming nine space shuttle and six Titan IV launches annually) [*Prather et al.*, 1990a; *Jones et al.*, 1995; *Jackman et al.*, 1996].

Paper number 2001JD900022.
0148-0227/01/2001JD900022$09.00

Since these studies, the question has been raised concerning whether or not alumina emissions could lead to an additional ozone depletion. Alumina particles could promote chlorine activation via the following reaction:

$$\text{(R1)} \qquad ClONO_2 + HCl \longrightarrow Cl_2 + HNO_3$$

with the relatively large temperature-independent reaction probability of 0.02 [*Molina et al.*, 1997]. Since the reaction probability of (R1) on background sulfate aerosol is at least an order of magnitude smaller at typical midlatitude lower stratospheric temperatures, it is important to check the possible chemical implications of (R1) for the ozone layer due to accumulation of alumina particles in the stratosphere from the SRM flights. *Jackman et al.* [1998], using the Goddard Space Flight Center (GSFC) two-dimensional (2-D) model, found that reaction (R1) on Al_2O_3 particles could deplete globally and annually averaged O_3 column by 0.01% (or by a factor of 2 less than that caused by chlorine emissions) for nine space shuttle and three Titan IV launches annually. They used a trimodal alumina particle distribution similar to that of *Brady and Martin* [1995] and simplified the gravitational sedimentation, accounting for it for each mode mean radius only.

Our study advances the previous work [*Jackman et al.*, 1998] by calculating the accumulation of alumina particles from the SRM launches with the Goddard Institute for Space Studies/University of California at Irvine (GISS/UCI) three-dimensional (3-D) chemistry-transport model (CTM), by including the effects of coagulation with background sulfate aerosol, by explicitly resolving the alumina size distribution in the calculation of gravitation sedimentation, and by using an updated size distribution for the alumina particles emissions. Also, a 3-D model can better represent the distribution of emissions from a large point source in the atmosphere than a 2-D model [*Holton et al.*, 1995]. We evaluate the chemical implications of the alumina particles for stratospheric ozone via reaction (R1) by using the atmospheric and Environmental Research (AER) 2-D model [*Weisenstein et al.*, 1998].

The structure of the paper is as follows. Section 2 discusses the emission scenario for the SRM launches, the assumed initial size distributions of alumina particles, and processes affecting their distribution in the atmosphere. Section 3 presents results for the alumina particle accumulation in the atmosphere, while section 4 discusses chemical implications of the atmospheric alumina for the ozone balance. The last section summarizes our results and outlines existing uncertainties regarding the potential role of solid particles on stratospheric ozone.

Table 1. Vertical Distribution of the Al_2O_3 Particle Source (in tons) for a Single Titan IV and Space Shuttle Launch and for a Scenario with Annual Launch Rate of Nine Space Shuttles and Four Titan IV.

Altitude, km	Titan IV	Space Shuttle	Scenario
15-20	11.6	21.1	236.3
20-25	9.2	16.7	187.1
25-30	9.1	16.5	184.9
30-35	7.4	13.5	151.1
35-40	7.2	13.1	146.7
40-45	5.7	10.4	116.4
45-50	4.8	8.7	97.5
Subtotal: 15-50	55	100	1120
Total: 0-50	165	360	3900

2. Model Representation of Al_2O_3 Emissions by SRMs

2.1. Emission Scenarios and Sensitivity Tests

The annual source of the Al_2O_3 particles from SRMs considered in this study includes nine space shuttle and four Titan IV launches from Cape Canaveral, Florida (29°N, 80°W). These launches deposit 3.9 kt/yr of alumina in the atmosphere, of which 1.12 kt/yr (900 and 220 t/yr from space shuttle and Titan IV, respectively) are deposited directly to the stratosphere (i.e., above 15 km) with the vertical distribution shown in Table 1. The Titan IV has a higher-altitude burn profile than the space shuttle. This scenario, usually used by the atmospheric modeling community [*WMO*, 1992], overestimates by 30% the actual SRM emissions during the last decade when the averaged annual rate was of 6.4 space shuttle and 2.2 Titan IV launches. We will show below that our results can be linearly scaled for the current or future launch scenarios. The tropospheric part (i.e., below 15 km) of the alumina emissions is not included in the calculations. Since we assume that alumina particles in the troposphere are removed by washout, tropospheric emissions cannot effectively penetrate to the stratosphere and accumulate there. Thus omission of the tropospheric alumina emissions will not affect our results.

In this study, the stratospheric emissions are assumed to be uniform throughout the year. To check whether or not this simplification could affect our results, we performed an additional sensitivity test by using a passive tracer with a source having a spatial distribution similar to that of the SRM fuel. In this test, we compare a pulsed emission injected every 40 days versus a uniform emission over the year with the same annual source strength. The difference between the two resulting tracer distributions on the monthly zonal mean concentrations (not shown here) is rather small (typically, less than 10%), justifying the uniform emission approach.

In this study, we assume that alumina particles do not interact with each other. This assumption provides an upper bound of the Al_2O_3 particle accumulation,

Table 2. Bin Sizes, Mean Radius, Al_2O_3 Source Strength , and Annually Zonally Averaged Surface Area Density (SAD) Over the Whole Stratosphere for Cases A, B, C, and D

Bin	Bin Edges, μm	Radius, μm	Source, t/yr	SAD, 10^{-6} $\mu m^2/cm^3$			
				Case A	Case B	Case C	Case D
1	0.025-0.04	0.03	2.4	19.4	18.7	6.04	192
2	0.04-0.06	0.05	4.5	23.4	22.2	10.8	228
3	0.06-0.10	0.08	4.3	14.6	12.9	8.87	132
4	0.10-0.16	0.13	1.5	3.44	2.44	2.16	25.1
5	0.16-0.25	0.20	0.1	0.19	0.08	0.08	0.8
first mode	0.025-0.25	...	12.8	61.03	56.32	27.95	577.9
6	0.25-0.40	0.32	1.5	1.22	0.78	0.78	3.67
7	0.40-0.64	0.51	5.2	2.66	1.44	1.44	6.77
8	0.64-1.02	0.81	12.6	4.05	1.77	1.77	8.32
second mode	0.25-1.02	...	19.3	7.93	3.99	3.99	18.76
9	1.02-1.61	1.28	37.3	7.38	2.27	2.27	1.87
10	1.61-2.56	2.03	125.6	15.6	3.16	3.16	2.60
11	2.56-4.06	3.23	295.0	23.8	2.66	2.66	2.19
12	4.06-6.45	5.12	399.5	20.7	1.22	1.22	1.01
13	6.45-10.00	8.13	230.5	7.93	0.22	0.22	0.18
third mode	1.02-10.00	...	1087.9	75.41	9.53	9.53	7.85
Total	0.25-10.00	...	1120.0	144.4	69.84	41.5	604.5

since possible coagulation between them would produce larger particles, resulting in their faster removal from the stratosphere by gravitational sedimentation. Assuming no interaction among the particles permits us to calculate the atmospheric distribution of each particle size separately, simplifying computations in the 3-D model. To determine the optimal number of bins with which to represent the alumina particle distribution, we performed a sensitivity study with the AER 2-D aerosol model [*Weisenstein et al.*, 1997]. The standard volume-doubling binning from this model uses 26 bins to represent the radius range from 0.025 to 8 μm. We calculated steady state aerosol distributions by using the 2-D model with the space shuttle Al_2O_3 source using 26 bins, and by using the 13 bins shown in Table 2 (using volume-quadrupling binning). We found the 13-bin solution to agree well with the 26-bin solution; so we adopted these 13 bins for the 3-D calculations.

The alumina emitted in the stratosphere is distributed among the size bins according to the following:

$$n(r) = n_1 \times \exp(-r/0.016), \quad 0.025 < r \leq 0.25\ \mu\text{m}$$

$$n(r) = n_2 \times \exp(-r/0.319), \quad 0.25 < r \leq 1\mu\text{m} \qquad (1)$$

$$n(r) = n_3 \times \exp(-r/1.25), \quad 1\ \mu\text{m} < r;$$

here $n(r)$ is the alumina particle distribution (in particles/(cm^3 μm) at radius r (in microns). In our 13-bin size distribution used in this study, the distribution in the first five bins is defined by the small mode; the next three bins, the medium mode; and the last five bins, the large mode. Equation (1) is mentioned by *Beiting* [1997], who parameterized the observed alumina particles by a trimodal distribution. The lognormal distribution of *Beiting* [1997] allows an overlap between the modes. We assume no overlap between different modes and switch from one to another n_i and r_i going between these modes. One can uniquely define the size distribution of alumina particles once their total concentration is given and the n_1/n_2 and n_2/n_3 ratios are known. In this study we apply $n_1/n_2 = 46{,}500$ and $n_2/n_3 = 10.3$ according to *Beiting* [1997]. Assuming that the density of alumina particles is size independent, the mass partitioning between small ($0.025 \leq r < 0.25$ μm), medium ($0.25 \leq r < 1$ μm), and large ($r > 1$ μm) modes is 1.1%, 1.7%, and 97.2%, respectively. The fourth column in Table 2 reflects this mass partitioning according to radius. In section 3 we discuss the importance of the size distribution for our results. Normalizing this size distribution by the total alumina mass emitted to the stratosphere per year ($S = 1.12$ kt/yr) and knowing the assumed size distribution and density of alumina particles ($\rho = 1.7$ g/cm^3), one can find the source function of the alumina particles according to the following equations:

$$S = \sum_{j=1}^{j=13} S_j \qquad (2)$$

$$S_j = \frac{4\pi}{3} \rho f_i \int_{\Delta r_j} r^3 \exp(-r/r_i)\, dr. \qquad (3)$$

Our calculations show that f_i equals 5.27×10^{25}, 1.13×10^{20}, and 1.17×10^{19} particles/(μm×yr) for the small ($i = 1$), medium ($i = 2$), and large ($i = 3$) modes, respectively. Once the mass of alumina emitted is distributed, we assume that particles in each bin have the same radius equal to the mean radius in this bin.

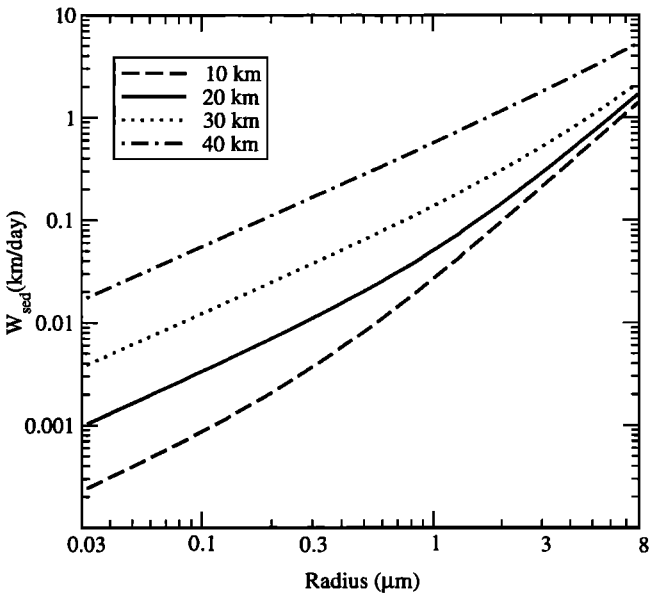

Figure 1. Zonally and annually averaged sedimentation velocity (in kilometers per day) of the Al_2O_3 particles at 28°N as a function of the particle size at altitudes of 10, 20, 30 and 40 km.

2.2. Relevant Atmospheric Processes

We transport 13 passive noninteracting tracers in the 3-D model representing the evolution of the particle distributions in the 13 bins. It is assumed that particles in each bin have the same size. The following three cases are considered: case A, in which the only removal is tropospheric washout, simulated by instantaneous removal in the lowest three model layers (i.e., below ~2 km); case B, in which, additionally, gravitational sedimentation is included; and case C, which is the same as B, plus coagulation with the background sulfate aerosol. As a sensitivity study, we also consider case D, which is similar to case B with a different emitted mass fractionation of alumina (EMFA). The sedimentation velocity w of a spherical particle with radius r and density ρ in the air with viscosity η and molecular mean free path λ is calculated following *Kasten* [1968] according to:

$$w = \frac{2\rho r^2 g}{9\eta}[1 + \frac{\lambda}{r}(1.249 + 0.42e^{-0.87r/\lambda})]; \quad (4)$$

here g is the acceleration due to gravity. Air viscosity is a function of ambient temperature, while molecular mean free path depends on both temperature and ambient pressure. Figure 1 shows w as function of radius at altitudes of 10, 20, 30, and 40 km at 29°N for the annually averaged conditions from the GISS/UCI CTM. It is clear that the sedimentation velocity is very sensitive to the radius of Al_2O_3 particles and increases with altitude owing to the reduction of viscosity and increase of λ. Indeed, the sedimentation velocity is about 90 times larger at 40 km than at 10 km for r = 0.03 μm. In general, particles larger than 1-μm radius are rapidly removed from the stratosphere, while smaller particles ($0.1 < r < 1$ μm) are also affected by the sedimentation at high altitudes. For particles with radius smaller than 0.1 μm, sedimentation plays a negligible role in their removal from the lower stratosphere.

In case C, we investigate the coagulation loss of Al_2O_3 particles with ambient sulfate aerosol, which is described in our model by:

$$\frac{\partial n_i}{\partial t} = n_i \sum_{k \geq i} K_{ik} n_k^{sul}, \quad (5)$$

here n_i is the concentration of alumina particles in the ith bin, K_{ik} is the collision rate between bins i and k [*Yue and Deepak*, 1979], and n_k^{sul} is the concentration of the ambient sulfate aerosol in the kth bin according to the nonvolcanic calculation from the AER 2-D model [*Weisenstein et al.*, 1997]. We assume in equation (5) that alumina particles coagulate only with sulfate particles of equal or larger size, ensuring their complete coating by the H_2SO_4/H_2O mixture. Once coating has occurred, the alumina particle is removed from our calculations. Case C should be considered as a sensitivity study of our results to coagulation of alumina particles with background sulfate aerosol. However, *Molina et al.* [1997] suggest that the alumina aerosols probably remain uncoated throughout most of their residence time in the stratosphere.

Figure 2 shows the coagulation removal rate (left vertical axis) and the $1/e$-folding time (right vertical axis) of the alumina particles as a function of their radius at 29°N at altitudes of 10, 20, and 30 km. The fastest removal occurs for the smaller particles because of their high mobility, which increases their collision

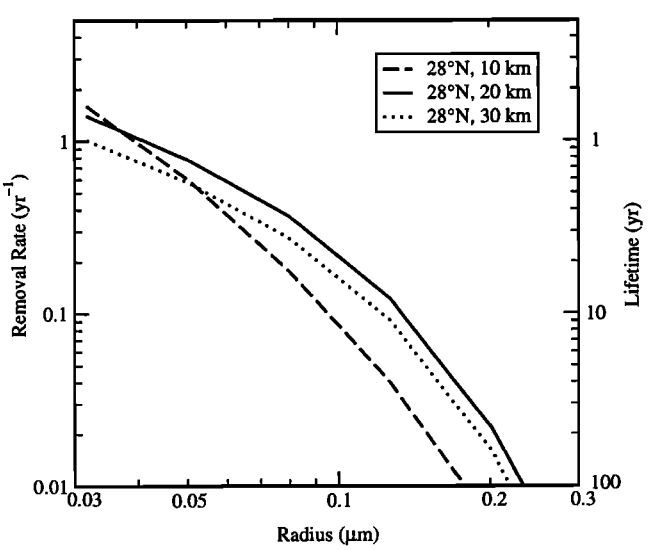

Figure 2. Zonally and annually averaged removal rate (in yr^{-1}, left vertical axis) and $1/e$-folding time (in years, right vertical axis) of the Al_2O_3 particles due to coagulation with background sulfate aerosol at 28°N as a function of particle size at altitudes of 10, 20, and 30 km.

frequency with the ambient sulfate aerosol. Thus only small (i.e., with $r < 0.1$ μm) alumina particles are effectively removed owing to coagulation, while the larger particles remain unaffected. Also, the removal rate is fastest where the ambient sulfate aerosol particle concentrations are larger (i.e., 10 and 20 km) and slower at higher altitudes, where little sulfate aerosol is available. The results shown in Figure 2 correspond to the background sulfate aerosol distribution from the AER 2-D model. For volcanic conditions it is reasonable to anticipate a faster removal rate of alumina particles from the global stratosphere by about an order of magnitude. Possible coagulation between alumina particles themselves (which is ignored in this study) could not affect our results significantly, since their concentration on the global scale is about a 1000 times less than that of the background sulfate aerosol.

3. Accumulation of Al_2O_3 Particles in the Atmosphere

The GISS/UCI 3-D CTM is used to investigate alumina particle accumulation in the atmosphere. We use the version of the model with a resolution of 7.83° in latitude, 10° in longitude, and 21 levels from the surface up to 0.0022 hPa. Horizontal binning is equidistant, while there are nine σ levels from the surface up to 100 hPa, with 12 additional levels above 100 hPa. The bottom nine layers are σ layers with the pressure at their edges defined as $p = \sigma \times (p_{\text{surface}} - 100\ \text{hPa}) + 100\ \text{hPa}$ with σ = 1., 0.973, 0.938, 0.887, 0.788, 0.633, 0.460, 0.278, 0.117, 0. The top 12 layers (above 100 hPa) are at fixed pressure levels, with pressure at the level edges equal to 46.41, 21.54, 10.00, 4.64, 2.15, 1.00, 0.46, 0.22, 0.100, 0.0466, 0.0215, and 0.0022 hPa. The advection scheme [*Prather*, 1986], which conserves second-order moments of the tracer distribution, is used in the model. The only diffusion included in the model is the horizontal mixing attributed to convection in the troposphere. The 3-D CTM is driven by the meteorological fields from the GISS-II general circulation model (GCM) with 23 layers. The lower 20 layers of the GCM and CTM are the same, while the top three layers in the GCM have been combined into a single layer to drive the 21-layer CTM. We apply the meteorological fields generated by the GISS GCM every 8 hours for 365 days. These wind fields are repeated every model year. This version of the model is described in detail by *Prather et al.* [1990b]. This model has been used to address a variety of atmospheric issues: the dynamical dilution of the Antarctic ozone hole [*Prather et al.*, 1990b]; the impact of SRM chlorine emissions on the ozone layer [*Prather et al.*, 1990a]; the seasonal evolution of N_2O, O_3, and CO_2 [*Hall and Prather*, 1995]; and tracer-tracer correlation in the stratosphere [*Avallone and Prather*, 1997].

A simple measure of the alumina particle accumulation in the atmosphere is its total burden. Results of the 3-D CTM calculations are presented in the third column of Table 3, which shows 3.02, 0.32, 0.31, and 0.755 kt of alumina in the global atmosphere for cases A, B, C, and D, respectively. Knowing the total stratospheric burden and the stratospheric source strength, one can calculate the global stratospheric lifetime (i.e., a steady state stratospheric burden divided by the stratospheric source) for the alumina emissions as 2.69, 0.29, 0.28, and 0.67 years for cases A, B, C, and D, respectively. The global atmospheric lifetime of alumina is about 3.5 times less (i.e., in the range 0.79-0.08 year) than the global stratospheric lifetime, since most of the alumina is accumulated in the stratosphere and the atmospheric alumina source is about 3.5 times larger. The lifetime of the alumina particles as a function of their radius is shown in Figure 3. Since washout and transport in the model are independent of size, all particles have the same residence time in case A. Figure 3 and Table 3 demonstrate that gravitational sedimentation is a major factor reducing the residence time of alumina particles in the atmosphere. Because less than 3% of the emitted alumina is in particles with radius of less than 1 μm, coagulation of alumina with background sulfate aerosol is unimportant for its total burden. However, coagulation is important for the surface area density (SAD) perturbations. Indeed, according to Tables 2 and 3, the differences between cases B and C for the total burden and SAD are about 3% and 40%, respectively. The large difference in SAD for these cases comes from the first four bins. These results demonstrate a well-known fact that smaller particles contribute more efficiently to the

Table 3. Cases Considered in This Study, Total Global Accumulation and Stratospheric Lifetime τ of Alumina Particles, Global Ozone Depletion, and the Ozone Depletion Potential (ODP) of Alumina Particles Based on the Total Mass of Alumina Emitted Into the Atmosphere

Case	Description	Burden, kt	τ, yrs	ΔO_3, 10^{-3}%	ODP
A	washout only	3.024	2.69	5.5	0.08
B	A + sedimentation	0.322	0.29	2.8	0.04
C	B + coagulation	0.311	0.28	2.1	0.03
D	B + BM95 EMFA[a]	0.755	0.67	24.7	0.35

[a]Case D is similar to case B with the emitted mass fractionation of alumina (EMFA) taken from [*Brady and Martin*, 1995].

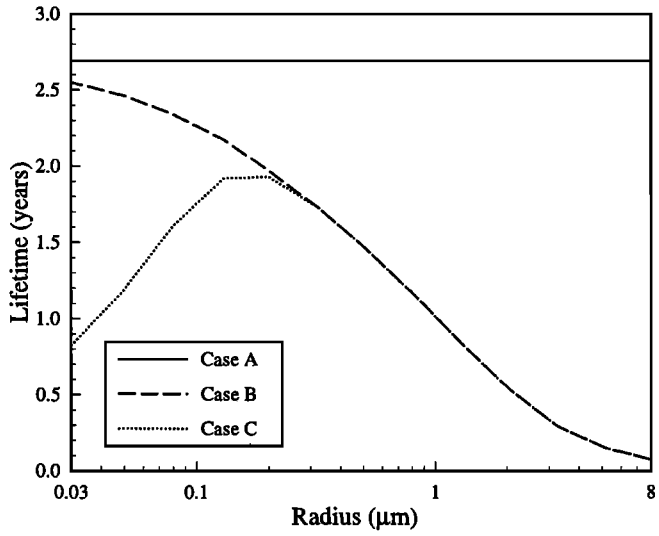

Figure 3. Annually average lifetime (in years) of the Al_2O_3 particles as a function of particle size integrated over the global atmosphere. Solid curve, case A (washout only); dashed curve, case B (sedimentation only); dotted curve, case C (sedimentation and collision removal). Calculation is performed by using size bins as specified in Table 2.

SAD than larger particles for the same amount of mass. Table 2 compares contributions of the different modes of alumina emissions to SAD perturbations. Alumina emissions in the smallest mode are about 20 and 500 times more efficient per unit mass in contributing to the SAD than those in the medium and large modes, respectively.

Since the rates of heterogeneous reactions are proportional to the surface area density, we calculate a distribution of alumina particle SAD to evaluate chemical implications of their accumulation in the stratosphere. In the 3-D CTM the mass mixing ratio of alumina particles is advected. Knowing the distribution of the alumina mass mixing ratio $m_i(z, \varphi, \chi)$ in the ith bin as a function of altitude z, latitude φ, and longitude χ, one can obtain the SAD distribution as

$$\mathrm{SAD}(z, \phi, \chi) = 4\pi \sum_{j=1}^{j=13} {r_j}^2 n_j(z, \varphi, \chi); \qquad (6)$$

here $n_j(z, \varphi, \chi) = 3\ m_i(z, \varphi, \chi)/(4\pi r_j^3 \rho)$ is the concentration of alumina particles. Figure 4 shows the latitude-longitude distribution of the alumina SAD at 20-km altitude in January for case B. There are several major features of this distribution. First, values of the accumulated alumina SAD are at least a 1000 times less than those of the background sulfate aerosol. Second, most of the alumina (i.e., >90% at 20 km) is accumulated in the Northern Hemisphere. Third, alumina SAD has a rather zonally symmetric distribution in the stratosphere owing to the longer timescale for accumulation relative to that of zonal mixing. Since the results look almost zonally symmetric at other altitudes, too, the use of zonal mean SAD in the AER 2-D model to estimate the chemical effects of the SRM alumina emissions and perform additional sensitivity studies is easily justified.

Figure 5 shows the zonally and annually averaged latitude-altitude dependence of the alumina SAD for cases A, B, C, and D. For the EMFA from *Beiting* [1997], the strongest perturbation is obtained in the Northern Hemisphere with a maximum of 1.5×10^{-3} $\mu m^2/cm^3$ at 20 km for case A. The location of the maximum is shifted poleward from 29°N owing to the mixing along isentropes poleward and downward. The maximum values decrease to 7×10^{-4} $\mu m^2/cm^3$ and 3×10^{-4} $\mu m^2/cm^3$ for cases B and C, respectively, owing to a shorter residence time of alumina particles when gravitational sedimentation and scavenging by the background aerosol are included. Since gravitational sedimentation keeps the particles from rising high enough to be carried over the tropical upwelling and into the Southern Hemisphere, much less alumina is accumulated there in cases B and C.

Since the results of our study are sensitive to emitted mass fractionation of alumina (see discussion below), we show in Figure 5d the alumina SAD for case D with EMFA according to *Brady and Martin* [1995] (i.e., 12, 8, and 80% alumina by mass is emitted in the small, medium, and large modes, respectively, compared with 1.1, 1.7, and 97.2% in these modes by *Beiting* [1997], as shown in Figure 5b). The values of SAD in Figure 5d are about 4-5 times larger than those shown in Figure 5b. This increase of SAD is attributed to a longer residence time of smaller particles which are presented in a larger proportion in this scenario.

We show alumina mass density accumulation in Figure 6. The maximum perturbation of 0.9 ng/m^3 is obtained for case A near 20 km. The absolute values of the alumina mass density are about an order of magnitude smaller in cases B and C, and this fact is reflected in Table 3. The latitude of the maximum values for cases B and C is closer to the SRM launch location owing to the shorter lifetime of the emissions in these scenarios

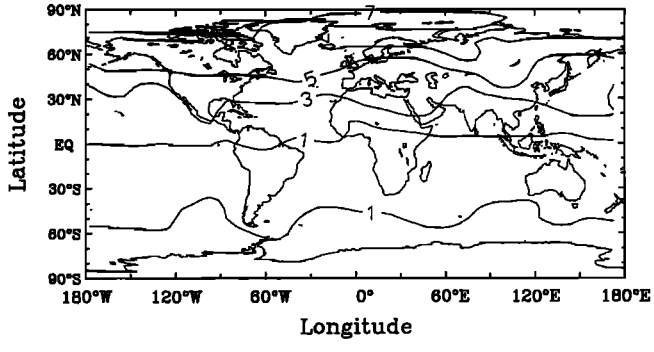

Figure 4. Latitude-longitude distribution of the Al_2O_3 SAD (in 10^{-4} $\mu m^2/cm^3$) at 20 km in January for Case B. The contours are from 1×10^{-4} to 7×10^{-4} $\mu m^2/cm^3$ with increment of 2×10^{-4} $\mu m^2/cm^3$.

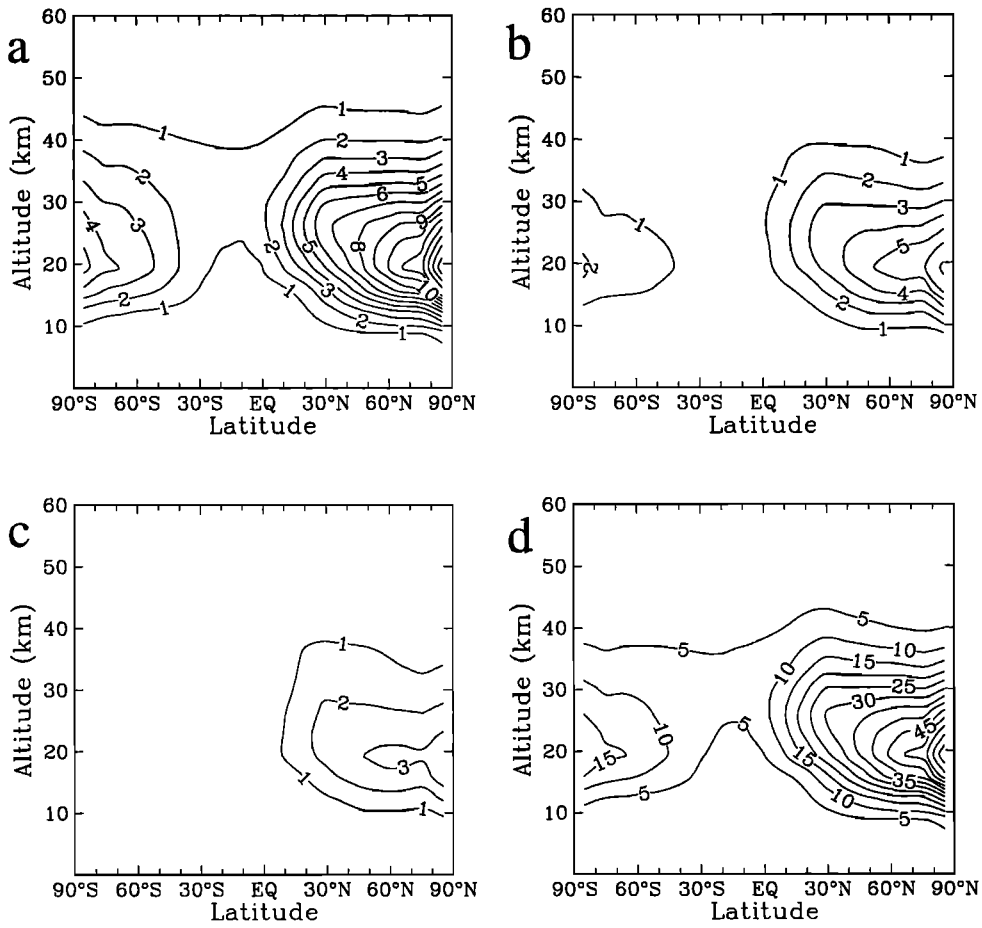

Figure 5. Annually zonally averaged latitude-altitude distribution of the Al_2O_3 surface area density (in 10^{-4} $\mu m^2/cm^3$) for (a) case A, (b) case B, (c) case C, and (d) case D. Contours are with increment of 10^{-4} and 5×10^{-4} $\mu m^2/cm^3$ in Figures 5a-5c and Figure 5d, respectively.

than in case A. Results for case D shown in Figure 6d have a maximum value of 0.18 ng/m^3 and are about twice as large as those in Figure 6b. To put these mass density values in perspective, one could compare them with those for the background sulfate aerosol and soot. The mass density derived from SAGE II data for April 1991 (just before the Pinatubo eruption and close to background levels) was about 100 ng/m^3 [*Yue et al.*, 1994]. Thus the alumina mass density is about 1000 times less in the more realistic cases B and C. On the other hand, the maximum value in cases B and C is an order of magnitude less than the ambient soot mass density (which has a maximum of 2 ng/m^3 at 10-12 km near 40°N [*Intergovernmental Panel on Climate Change (IPCC)*, 1999]).

Figures 5-6 allow us to estimate the effects of gravitational sedimentation and coagulation on the alumina SAD and mass density distribution. The difference between the Figures 5a/6a and Figures 5b/6b shows the role of gravitational sedimentation, while the difference between Figures 5b/6b and Figures 5c/6c shows the effects of coagulation, and the difference between Figures 5b/6b and Figures 5d/6d demonstrates the role of EMFA. The effects due to EMFA and sedimentation are more pronounced than those due to coagulation in the SAD and mass density distribution. The ratio of SAD to mass density provides some hints regarding alumina particle size distribution. For example, since the mass densities for cases B and C are almost identical while the SAD in case B is twice as large as in case C, we conclude that the difference originated in the smallest bins.

A very important source of uncertainty for our calculations is the size distribution of alumina particles emitted by the SRMs. In cases A-C we used the EMFA according to *Beiting* [1997], in which only 1.1% of total alumina mass is emitted in the small mode of the trimodal size distribution. *Brady and Martin* [1995] assumed that 12% of emitted alumina by mass is located in the small mode, i.e., a factor of 10 larger than that of *Beiting* [1997]. *Ross et al.* [1999] analyzed aircraft in situ samplings of the space shuttle and Titan IV wakes, which confirmed the trimodal size distribution of alumina particles. However, their results show that less than 0.05% of alumina emitted resides in the small mode (i.e., a factor of 20 and 240 less than that

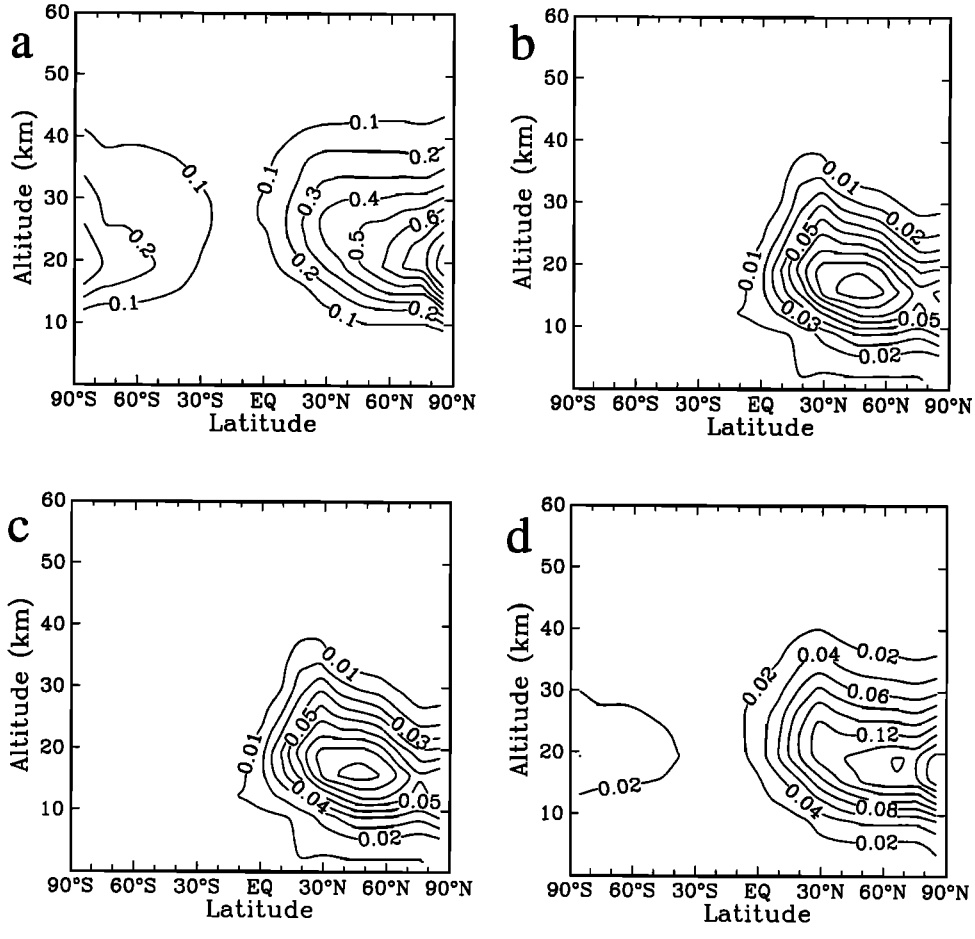

Figure 6. The same as in Figure 5, but for the Al_2O_3 mass density (in ng/m^3). Contours are with increment of (a) 0.1, (b-c) 0.01, and (d) 0.02 ng/m^3.

of *Beiting* [1997] and *Brady and Martin* [1995], respectively). The main reason for such big discrepancies is the fact that existing alumina particle measurements [*Strand et al.*, 1981; *Zolensky et al.*, 1989; *Cofer et al.*, 1991] are very sparse, obtained at different altitudes with different limited portions of the size distribution, and under different atmospheric conditions (i.e., in the aged SRM plumes versus ambient air). The lack of systematic measurements of alumina particles in the size range 0.01-1 μm at different latitudes and altitudes in the ambient stratosphere makes validation of our 3-D model calculations practically impossible.

To quantify uncertainties of initial alumina mass partitioning among the three modes in terms of the steady state SAD perturbation, the following calculations could be performed for any EMFA without additional 3-D model runs. One can use the values of 4.4 $\times$ 10^{-6}, 2.1i $\times$ 10^{-7}, and 8.8 $\times$ 10^{-9} μm^2/cm^3/(t/yr), obtained by dividing the SAD perturbation (sixth column) by the source (fourth column) in each mode from Table 2 for case B. Assuming the same launch scenario and using the *Brady and Martin* [1995] alumina mass partitioning, one can estimate an SAD increase of 5.9 $\times$ 10^{-4}, 1.9 $\times$ 10^{-5}, and 7.9 $\times$ 10^{-6} μm^2/cm^3 in the small, medium, and large modes, or 6.2 $\times$ 10^{-4} μm^2/cm^3 in three modes. The last value is almost an order of magnitude larger than that shown in the bottom line of the sixth column in Table 2 and is in a good agreement with the results shown at the bottom of the last column in Table 2.

4. Ozone Response to Alumina Particle Emissions

We use the AER 2-D model to estimate the chemical consequences of alumina particle accumulation in the stratosphere. We apply the 2-D model instead of the 3-D CTM because the distribution of the alumina particles in the stratosphere is almost zonally symmetric and the AER 2-D model has a developed and well-documented stratospheric ozone chemical module [*Weisenstein et al.*, 1998] and has been used in many previous intercomparison and assessment studies of ozone depletion [e.g., *WMO*, 1992; *Park et al.*, 1999; *IPCC*, 1999]. The vertical and horizontal resolutions of the model used in this study are 1.2 km and 9.5°, respectively. The $ClONO_2 + HCl \rightarrow Cl_2 + HNO_3$ reaction on alumina particles with $\gamma = 0.02$ [*Molina et al.*, 1997]

has been added to the comprehensive list of the photochemical and heterogeneous reactions in the model.

Figure 7 shows ozone column response to the SRM emissions for chlorine emissions only (Figure 7a) and for chlorine and alumina emissions according to case B (Figure 7b), case C (Figure 7c), and Case D (Figure 7d). These responses are defined as the percent difference between two model runs with and without emissions (i.e., background atmosphere). When only chlorine emissions are considered, the maximum ozone column depletion is equal to 0.05%. For cases B and C, ozone responses show maximum values of about 0.06%. Maximum ozone perturbation for case A is about 0.07% (not shown here). The latitudinal and seasonal behavior of the ozone response is similar in all cases, showing strongest perturbation during spring in the northern polar latitudes and practically no perturbation in the Southern Hemisphere. The globally averaged ozone column depletions are 0.0123%, 0.0151%, 0.0144%, and 0.034% for the cases shown in Figures 7a, 7b, 7c, and 7d, respectively. For such small perturbations of ozone, the effects due to chlorine and alumina emissions are additive. Thus the globally annually averaged ozone responses to alumina emissions alone are equal to -0.0028%, -0.0021%, and -0.0247% for cases B, C, and D, respectively.

Our ozone response to chlorine emissions only (-0.0123%) is somewhat smaller than that (-0.023%) of *Jackman et al.* [1998], which could be explained by different circulations and a faster washout in the AER 2-D model, leading to a smaller chlorine accumulation in the stratosphere. Indeed, the peak values of SRM-emitted chlorine are 8 and 12 pptv in the AER and GSFC 2-D models, respectively. Our results for case D could be compared with those of *Jackman et al.* [1998]. C.H. Jackman kindly provided the Al_2O_3 SAD used in the *Jackman et al.* [1998] study. His values show a maximum of 2×10^{-3} $\mu m^2/cm^3$ at 10-16 km poleward of 45°N, which is a factor of 2 smaller than our values shown in Figure 5d. The detailed analysis of this difference is beyond the scope of this paper. Here we would like to offer the following possible explanation. First, the circulations in the models are different. Second, the simplified calculations [*Jackman et al.*, 1998]

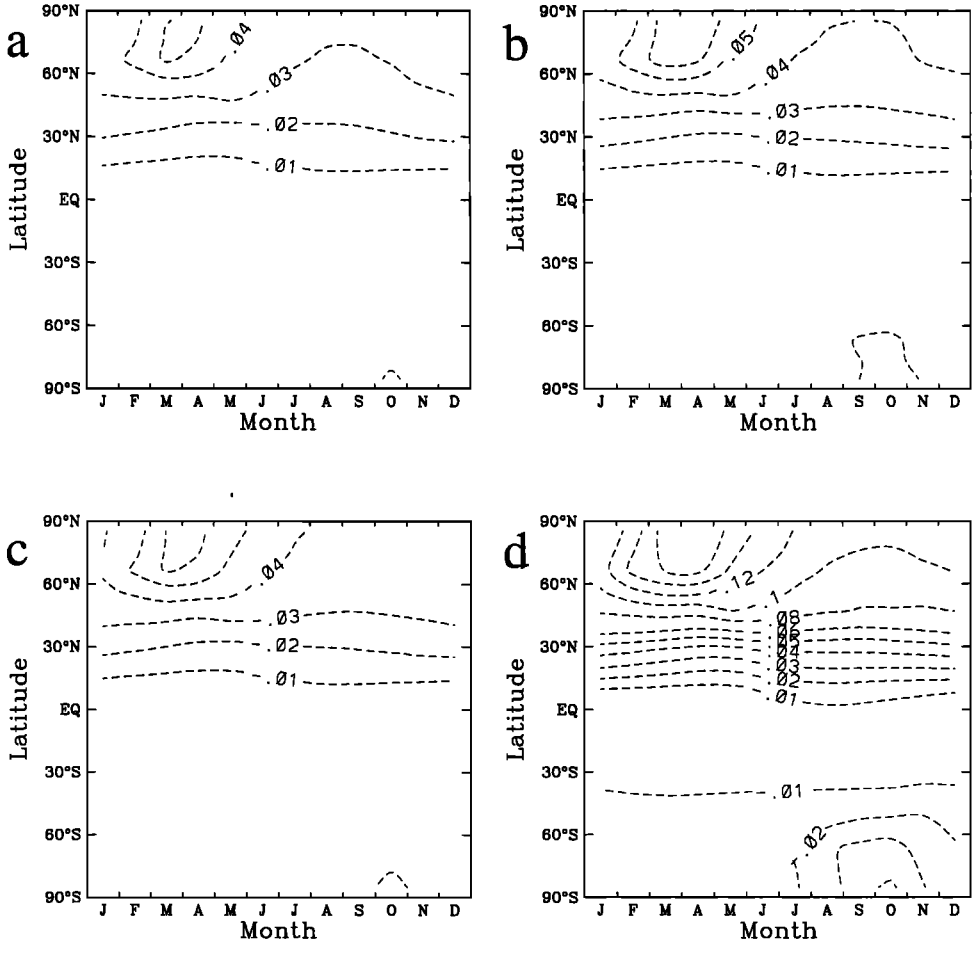

Figure 7. Depletion of the ozone column (in percent) to the SRM emissions including (a) chlorine only, (b) chlorine plus Al_2O_3 from case B, (c) case C, and (d) case D as a function of latitude and season. Contour are with increment of 0.01% between 0 and -0.06% and 0.02% from -0.6% to -0.16%.

assume that the size distribution within each mode remains the same. In reality, the final size distribution in each mode is biased toward smaller particles because of gravitational sedimentation and differs substantially from the initial size distribution of the emitted particles. Thus the *Jackman et al.* [1998] study likely overestimated the averaged sedimentation velocity in each mode and underestimated the amount of the alumina accumulated in the stratosphere.

Our ozone response to alumina emissions in case D (0.0247%) is more than twice as large as the ozone depletion of -0.01% obtained by *Jackman et al.* [1998]. However, this difference can be explained by the larger Al_2O_3 SAD accumulated in our calculations, providing a similar sensitivity of the ozone depletion per unit of alumina SAD accumulated. Because the ozone perturbations are very small, they can be linearly scaled to predict the impact of different rates of SRM launches than that adopted here, if the launch location and vertical distribution of the emissions remain the same as in this study.

The ozone depletion potential (ODP) of a compound is defined as the ratio of the steady state global ozone reduction due to emission of the compound divided by its steady state annual emission to the same mass of CFC-11 [*WMO*, 1992]:

$$\mathrm{ODP}(Al_2O_3) = \frac{\frac{\text{global } O_3 \text{ loss due to } Al_2O_3}{\text{emission rate of } Al_2O_3}}{\frac{\text{global } O_3 \text{ loss due to CFC-11}}{\text{emission rate of CFC-11}}} \quad (7)$$

According to the AER 2-D model calculations, 52.8 kt/yr of CFC-11 emissions cause a global ozone steady state depletion of 0.993%. On the other hand, 3.9 kt/yr alumina emissions cause 0.0055%, 0.0028%, and 0.0021% global ozone depletion for cases A, B, and C, respectively. Note that we use the total (i.e., tropospheric and stratospheric) alumina source for the ODP(Al_2O_3) calculations, while only its stratospheric part (i.e., above 15-km altitude) is used to calculate the alumina accumulation in the stratosphere. The resulting values of ODP(Al_2O_3) are 0.08, 0.04, and 0.03 for cases A, B, and C, respectively. These values are relatively high in comparison with that of other freons but several times less than the steady state ODP value of 0.14 corresponding to the space shuttle emissions of HCl [*Ko et al.*, 1994]. However, the ODP(Al_2O_3) is very sensitive to the emitted alumina mass fractionation. As we mentioned above, for the *Brady and Martin* [1995] EMFA, our model shows globally annually averaged ozone depletion of 0.037% (or 0.0247% due to alumina emissions alone), which is translated to the ODP(Al_2O_3) of 0.35. In situ measurements of the alumina particle size distribution in the SRM plumes are urgently required to determine unambiguously what fraction of emitted alumina are located in the small mode (i.e., with radii of <0.25 μm).

There are other possible heterogeneous reactions on alumina particles, for example, ozone and CFC-12 decomposition. However, these reactions were not included in our 2-D model calculations because their reaction probabilities are very low. For example, they are less than 10^{-9} [*Hanning-Lee et al.*, 1996] and equal to 2×10^{-5} [*Robinson et al.*, 1994] for the ozone and CFC-12 decompositions, respectively. *Jackman et al.* [1998] included the CFC-12 decomposition in his model and got a tiny global ozone change ($+4.2 \times 10^{-5}$%). Other possible decomposition reactions of $CFCl_3$, CF_3Cl, and CF_2Br_2 mentioned by *DeMore et al.* [1997] have reaction probabilities of order 10^{-5} and thus are also unimportant. However, it is not yet clear whether other important reactions could occur on alumina surfaces which are overlooked in our study. More laboratory studies are necessary to address this possibility.

5. Conclusions and Outlook

For the first time the global accumulation and size distribution of the alumina particles from the SRM emissions are investigated by using a 3-D CTM. A 3-D model is most appropriate for calculation of the accumulation of SRM alumina, since alumina emissions represent large point sources in the middle world, a situation where 2-D models are suspect [*Holton et al.*, 1995]. Our study provides important information regarding the accumulation of SRM alumina in the atmosphere with detailed information about the size distribution of alumina particles. Using the EMFA according to *Beiting* [1997] as a baseline case and including tropospheric washout and gravitational sedimentation, we obtain a global distribution of alumina SAD and mass density with annually zonally averaged maximum values up to 7×10^{-4} $\mu m^2/cm^3$ and 0.09 ng/m^3, respectively, near 20 km in the Northern Hemisphere in case B. These values are at least a 1000 times less than those of background sulfate aerosol. The caveat associated with these values is their very high sensitivity to initial mass partition of alumina emissions among the three modes. This partitioning is poorly known currently, and estimates of the alumina mass in the small mode differ by a factor of 240 [*Brady and Martin*, 1995; *Ross et al.*, 1999]. The values of SAD reported in this study could be larger by an order of magnitude if more alumina mass is emitted in small bins (i.e., at $r < 0.25$ μm).

Alumina particles could affect the ozone layer via reaction (R1). This impact is rather small ($2.8i \times 10^{-3}$ % in the global annually averaged column in case B). However, on a per unit mass emitted basis, alumina emissions from SRMs are quite effective in depleting ozone, with ODPs in the range of 0.03-0.08. Again, these results are valid for the EMFA according to *Beiting* [1997]. If the *Brady and Martin* [1995] EMFA is used, the ODP(Al_2O_3) value is equal to 0.35. Such a high value urges detailed in situ measurements characterizing the alumina particle size distribution emitted by SRMs. Comparison of our ozone response with that of *Jackman et al.* [1998] shows a larger perturbation

in our study due to the larger alumina accumulation in the stratosphere. However, the ozone response per unit of alumina SAD is similar in ours and *Jackman et al.*'s [1998] studies.

The contribution of additional SRMs could be roughly estimated by scaling of the alumina deposited by these rockets in the stratosphere. The most important missing SRM source in this study is the Ariane 5 launches, which contribute about 57 tons of alumina per launch into the stratosphere. Assuming 10 launches of Ariane 5 per year [*Jones et al.*, 1995], one can get a source of about 570 t/yr, or about half of what was considered in our study. If 8 launches of each Atlas II and Delta II rockets occur annually, an additional 27 tons and 60 tons of alumina, respectively, will be injected into the stratosphere. Thus a total source of approximately 660 t/yr is missing in our study. As a first guess, our results in Figures 5-6 should be scaled up by a factor of $(1120 + 660)/1120 \approx 1.6$ when the Arian 5, Atlas II, and Delta II launches with the mentioned launch frequencies and fractionation of alumina particle as in paper by *Beiting* [1997] are taken into consideration. An important caveat associated with this scaling is that the various SRMs are launched from different latitudes. In particular, the Ariane 5 is launched from Kourou, French Guiana (5.2°N, 52.8°W), while Atlas II and Delta II can be launched from Vandenberg Air Force Base (34.8°N, 120.6°W).

Our study does not include sources of alumina such as meteorites or deorbiting spacecraft. The impact of the alumina particles from meteorites and orbital debris is poorly known, deserves a special study, and is beyond the scope of this paper.

Summarizing our results, we conclude that the fractionation of the SRM alumina particles emitted and their reactivity are the most important parameters for calculating ozone impacts, and they are currently very poorly understood. Our results show that for such small ozone perturbations, the global-averaged ozone depletion can be linearly scaled with the accumulated alumina SAD. On the basis of current knowledge, we conclude that the environmental impact of alumina emissions in the stratosphere is small on the global scale for the present SRM launch frequency. This issue should be revisited if further research discovers the existence of faster ozone-depleting reactions on alumina surfaces or finds that most of the alumina is emitted in the range 0.01-0.1 μm. Large increases in the SRM launch frequency might also warrant additional impact studies.

Acknowledgments. This work is sponsored by the Space and Technology Division of TRW, Inc., under a contract (F09603-95-D-0176-0007) from the U.S. Air Force Space and Missile Systems Center Environmental Management Division (John R. Edwards and Dan Pilson). Work at AER, Inc., is also supported by NASA ACMAP (NAS5-97039). Work at UCI is supported by grants from NASA's Earth Science Office. We are grateful to Charles Jackman (GSFC) for providing unpublished results related to his 1998 study and very valuable discussions. We also benefited from discussions with Charles Kolb (Aerodyne Research, Inc.). We gratefully acknowledge the helpful comments of the anonymous reviewers and Valerie Lang (Aerospace Corporation).

References

Avallone, L. M., and M. J. Prather, Tracer-tracer correlations: Three-dimensional model simulations and comparisons to observations, *J. Geophys. Res., 102,* 19,233-19,246, 1997.

Beiting, E. J., Solid rocket motor exhaust model for alumina particles in the stratosphere, *J. Spacecr. Rockets, 34,* 303-310, 1997.

Brady, B. B., and L. R. Martin, Modeling solid rocket booster exhaust plumes in the stratosphere using SURFACE CHEMKIN, Techn. Rep. *TR-95(5231)-9,* Aerospace Corp., El Segundo, Calif., 1995.

Cofer, W. R., III, G. C. Purgold, E. L. Winstead, and R. A. Edahl, Space shuttle exhausted aluminum oxide: A measured particle size distribution, *J. Geophys. Res., 96,* 17,371-17,376, 1991.

DeMore, W. B., et al., Chemical kinetics and photochemical data for use in stratospheric modeling, evaluation 12, *JPL Publ. 97-4,* Jet Propul. Lab., Pasadena, Calif., 1997.

Hall, T. M., and M. J. Prather, Seasonal evolution of N_2O, O_3, and CO_2: Three-dimensional simulations of stratospheric correlations, *J. Geophys. Res., 100,* 16,699-16,720, 1995.

Hanning-Lee, M. A., B. B. Brady, L. R. Martin, and J. A. Syage, Ozone decomposition on alumina: Implications for solid rocket motor exhaust, *Geophys. Res. Lett., 23,* 1961-1964, 1996.

Holton, J. R., P. H. Haynes, M. E. McEntyre, A. R. Douglass, R. R. Rood, and L. Pfister, Stratosphere-troposphere exchange, *Rev. Geophys., 33,* 403-439, 1995.

Intergovernmental Panel on Climate Change (IPCC), Aviation and the Global Atmosphere, Cambridge Univ. Press, New York, 1999.

Jackman, C. H., et al., Space shuttle's impact on the stratosphere: An update, *J. Geophys. Res., 101,* 12,523-12,529, 1996.

Jackman, C. H., D. B. Considine, and E. L. Fleming, A global modeling study of solid rocket aluminum oxide emission effects on stratospheric ozone, *Geophys. Res. Lett., 25,* 907-910, 1998.

Jones, A. E., S. Bekki, and J. A. Pyle, On the atmospheric impact of launching the Ariane 5 rocket, *J. Geophys. Res., 100,* 16,651-16,660, 1995.

Kasten, F., Falling speed of aerosol particles, *J. Appl. Meteorol., 7,* 944-947, 1968.

Ko, M. K. W., N. D. Sze, and M. J. Prather, Better protection of the ozone layer, *Nature, 367,* 505-508, 1994.

Molina, M. J., L. T. Molina, R. Zhang, R. F. Meads, and D. D. Spencer, The reaction of $ClONO_2$ with HCl on aluminum oxide, *Geophys. Res. Lett., 24,* 1619-1622, 1997.

Park, J. H., M.K.W. Ko, C.H. Jackman, R.A. Plumb, J.A. Kaye, and K.H. sage, Models and measurements intercomparison II, *NASA/TM-1999-209554,* 494 pp., 1999.

Prather, M. J., Numerical advection by conservation of second-order moments, *J. Geophys. Res., 91,* 6671-6681, 1986.

Prather, M. J., M. M. Garcia, A. R. Douglass, C. H. Jackman, M. K. W. Ko, and N. D. Sze, The space shuttle's impact on the stratosphere, *J. Geophys. Res., 95,* 18,583-18,590, 1990a.

Prather, M. J., M. M. Garcia, R. Suozzo, and D. Rind, Global impact of the Antarctic ozone hole: Dynamical

dilution with a 3-D CTM, *J. Geophys. Res., 95*, 3449-3471, 1990b.

Robinson, G.N., et al., Decomposition of halomethanes on α-alumina at stratospheric temperatures, *Geophys. Res. Lett., 21*, 377-380, 1994. (correction, *Geophys. Res. Lett., 23*, 317, 1994.)

Ross, M. N., P. D. Whitefield, D. E. Hagen, and A. R. Hopkins, In situ measurement of the aerosol size distribution in stratospheric solid rocket motor exhaust plumes, *Geophys. Res. Lett., 26*, 819-822, 1999.

Strand, L. D., J. M. Bowyer, G. Varsi, E. G. Laue, and R. Gauldin, Characterization of particles in the exhaust plume of large solid-propellant rockets, *J. Spacecr. Rockets, 18*, 297-305, 1981.

Weisenstein, D. K., G. K. Yue, M. K. W. Ko, N. D. Sze, J. M. Rodriguez, and C. J. Scott, A two-dimensional model of sulfur species and aerosols, *J. Geophys. Res., 102*, 13,019-13,035, 1997.

Weisenstein, D. K., M. K. W. Ko, I. G. Dyominov, L. Ricciardulli, G. Visconti, and S. Bekki, The effect of sulfur emissions from HSCT aircraft: A 2-D model intercomparison, *J. Geophys. Res., 103*, 1527-1547, 1998.

World Meteorological Organization(WMO), Scientific Assessment of Ozone depletion: 1991, Rep.25, Chap. 10, pp.10.1-10.12, Geneva, 1992.

Yue, G. K., and A. Deepak, Modeling of coagulation-sedimentation effects on transmission of visible IR laser beam in aerosol media, *Appl. Opt., 18*, 3918-3925, 1979.

Yue, G. K., L. R. Poole, P.-H. Wang, and E. W. Chou, Stratospheric aerosol acidity, density, and refractive index deduced from SAGE-II and NMC temperature data, *J. Geophys. Res., 99*, 3727-3738, 1994.

Zolensky, M. E., D. S. McKay, and L. A. Kaszor, A tenfold increase in the abundance of large solid particles in the stratosphere, as measured over the period 1976-1984, *J. Geophys. Res., 94*, 1047-1056, 1989.

M. Y. Danilin, M. K. W. Ko, R.-L. Shia, N. D. Sze, and D. K. Weisenstein, AER, Inc., 131 Hartwell Avenue, Lexington, MA 02421. (danilin@aer.com; ko@aer.com; rls@aer.com; nsze@aer.com; dkweis@aer.com)

J. J. Lamb, P. D. Lohn, and T. W. Smyth, TRW Space and Technology Division, One Space Park, Redondo Beach, CA 90278. (John.Lamb@trw.com, Pete.Lohn@trw.com, Tyrrel.Smyth@trw.com)

M. J. Prather, Department of Earth System Science, University of California, Irvine, CA 92697. (mprather@uci.edu)

(Received July 27, 2000; revised November 7, 2000; accepted January 11, 2001.)